Molecular Therapy
Methods & Clinical Development
Original Article

In vivo delivery of a fluorogenic antisense oligonucleotide into human leukocytes in a humanized mouse model system

Nathan B. Seidel,[1] Saurav S. Rout,[1] Beverly Z. Packard,[2,3] and Kerry J. Lavender[1,3]

[1]Department of Biochemistry, Microbiology and Immunology, College of Medicine, University of Saskatchewan, Saskatoon, SK S7N 5E5, Canada; [2]OncoImmunin, Inc., Gaithersburg, MD 20877, USA

Development of oligonucleotide-based therapeutics has been limited by the lack of effective *in vivo* delivery vehicles. We previously showed that the presence of an H-type excitonic dimer formed by the covalent binding of two fluorophores with significant transition dipoles on opposite ends of peptide or nucleic acid sequences of interest facilitated their delivery into live cells *in vitro*. Here, we evaluated delivery of a fluorogenic anti-sense oligonucleotide (ASO) complementary to β-actin (*ACTB*) mRNA into human leukocytes *in vivo* using a humanized mouse model. We observed delivery of the ASO into human leukocytes at a median of ≥94% in blood, spleen, bone marrow, and liver with half-lives of at least 72 h. Additionally, we detected the ASO in a significant proportion of human leukocytes within difficult-to-penetrate tissues such as brain and gut. The ASO localized to the perinuclear space within target cells and mediated reductions in bone marrow *ACTB* transcripts after a single intravenous injection. The delivery system described herein is a technology platform with the capacity for highly efficient systemic delivery of therapeutic oligonucleotides that will facilitate development of a new class of drugs for treatment of HIV and other pathologic conditions.

INTRODUCTION

Oligonucleotides have become essential tools in basic biomedical research and are currently used in a multitude of applications; however, their potential for highly specific oligonucleotide-based therapeutics has been limited by the lack of effective delivery vehicles. Delivery of polymers such as oligonucleotides into live cells has proven to be difficult in the absence of carriers such as lipids, e.g., liposomes and nanoparticles, or receptor-ligand conjugates, e.g., GalNAc-siRNAs/ASOs, where such polymers must cross the plasma membrane of individual cells without being trapped in endosomes.[1–3] An even more difficult problem is delivery of therapeutic oligonucleotides *in vivo* as additional barriers to target sequences exist.[4–7] This has been particularly true for infectious diseases such as HIV due to suboptimal delivery to hematopoietic cells such as $CD4^+$ lymphocytes.[8,9] Although antisense oligonucleotides (ASOs) and small interfering RNAs (siRNAs) have been "delivered" into cells *in vitro* and *in vivo* by various transfection methods, none has been shown to be without major drawbacks at the whole animal level.[4–7]

We have previously shown that by modifying a molecular design initially developed for delivering fluorogenic peptides into live cells to measure intracellular protease activities,[10–12] fluorogenic ASOs could be delivered into live cells *in vitro*. Specifically, we were able to inhibit HIV infection with several different ASO sequences targeting the non-translated region of the virus.[13,14] What has made delivery of both peptides and oligonucleotides into live cells possible has been the presence of an H-type excitonic dimer formed by the covalent binding of two fluorophores with significant transition dipoles on opposite ends of an amino acid or nucleic acid sequence of interest.[15,16] The H-type excitonic dimer has been shown to allow non-specific cellular entry via passive diffusion across plasma cell membranes.[12,17]

Using our previously developed delivery vehicle for the delivery of peptides and oligonucleotides into live cells *in vitro*,[15,16] we sought to evaluate the delivery of a fluorogenic, non-gapmer ASO bearing a complementary sequence to β-actin (*ACTB*) mRNA into human leukocytes in multiple tissues *in vivo* using a humanized immune system mouse model, specifically, C57BL/6 $Rag2^{-/-}\gamma c^{-/-}CD47^{-/-}$ triple knockout (TKO) mice that were humanized using the bone marrow, liver, and thymus (BLT) method.[18] The resultant TKO-BLT mice are highly reconstituted with human leukocyte subsets in both blood and tissues.[19] Our primary objective was to demonstrate the delivery of the *ACTB* ASOs to human leukocytes in the blood, bone marrow, liver, spleen, brain, and gut by quantitating the fluorogenic signal generated upon gene-target-specific

Received 25 April 2025; accepted 28 August 2025;
https://doi.org/10.1016/j.omtm.2025.101583.

[3]These authors contributed equally

Correspondence: Beverly Z. Packard, OncoImmunin, Inc., Gaithersburg, MD 20877, USA.
E-mail: bpackard@phiphilux.com
Correspondence: Kerry J. Lavender, Department of Biochemistry, Microbiology and Immunology, College of Medicine, University of Saskatchewan, Saskatoon, SK S7N 5E5, Canada.
E-mail: kerry.lavender@usask.ca

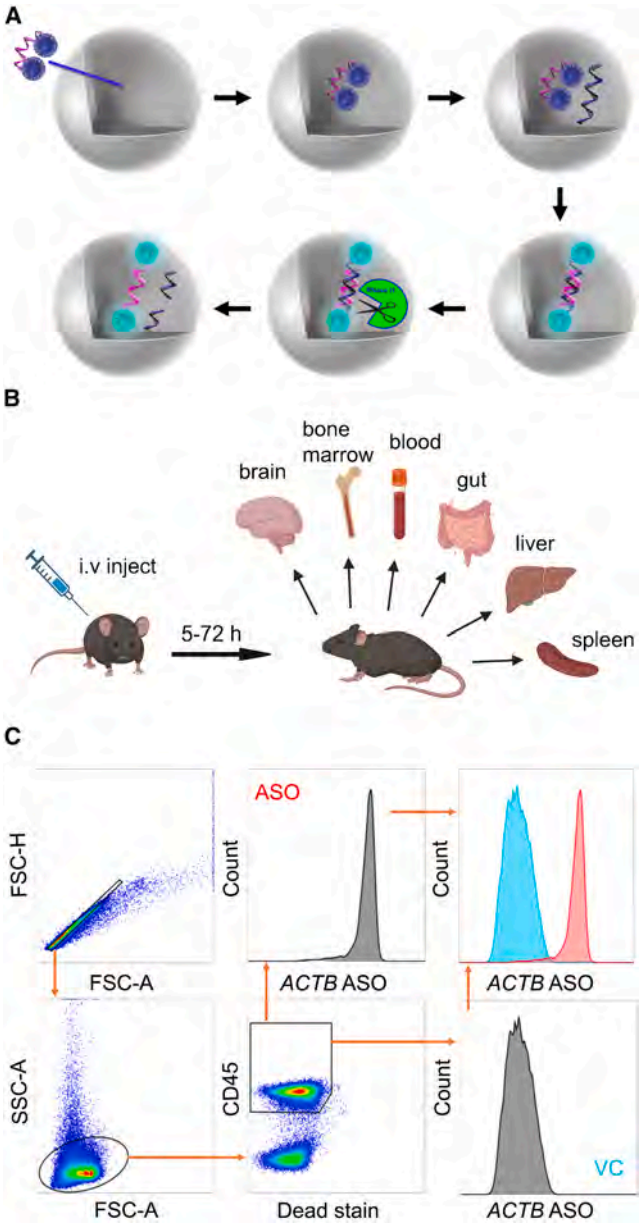

Figure 1. Assessment of homo-doubly labeled *ACTB* ASO delivery to cells and tissues *in vivo*

(A) Illustration of entry of a homo-doubly labeled ASO into a live cell and hybridization-dependent fluorescence dequenching leading to mRNA inhibition in the cell. In the upper left two panels, a double fluorophore (blue balls)-labeled ASO (antisense oligonucleotide sequence is in pink) enters a cell in a receptor-independent manner consistent with passive diffusion. Upon encountering a complementary sequence (dark blue helix), hybridization occurs resulting in a fluorescent signal as depicted in the upper right to lower right panels. If the cell contains an RNase in the cytoplasm, then the target mRNA sequence can be cleaved as shown in the lower left panel. (B) Homo-doubly labeled *ACTB* ASO injection into TKO-BLT humanized mice and tissue collection at 5, 24, 48, or 72 h. Image was produced with BioRender. (C) Representative flow cytometry plots gating on live human CD45$^+$ leukocytes and assessment of fluorescence within cells from treated (ASO) or vehicle control (VC) animals.

hybridization. Additionally, the potential for the functional knockdown of the *ACTB* message in human hematopoietic cells after a single ASO dose was briefly evaluated.

RESULTS

Experimental design

To evaluate the *in vivo* delivery of a fluorogenic ASO into human leukocytes, we designed a non-gapmer ASO that bore a fluorophore on each end of a complementary sequence of a known mRNA such that the fluorescence was largely quenched.[12,13,16] In this study, the homo-doubly labeled ASO sequence was complementary to the β-actin housekeeping gene (*ACTB*) such that when the probe enters a cell and encounters the *ACTB* mRNA, hybridization leads to dequenching of the fluorescence. The phosphorothioate linkages throughout the backbone provide for nuclease resistance, and therefore, the dequenched signal represents the intact ASO binding to a complementary sequence inside the cell. A diagram illustrating the mechanism is presented in Figure 1A where in the upper left two panels the two fluorophores are blue balls attached to an ASO, which is shown as a pink helix. Upon entry into the cell (gray ball with cutout) in a receptor-independent manner consistent with passive diffusion, the homo-doubly labeled ASO encounters a complementary sequence (dark blue helix), and this interaction leads to hybridization, resulting in a fluorescent signal as depicted in the lower panels. RNase activity in the cytoplasm such as host RNAase H1 or reverse transcriptase from HIV can then target the mRNA sequence, resulting in cleavage as shown in the lower left panel.

We delivered the homo-doubly labeled *ACTB* ASO intravenously to humanized TKO-BLT mice that support a highly reconstituted human immune system comprised of all the major human CD45$^+$ cell lineages dispersed systemically within the blood and tissues of the animals.[19] Doses of 0–2 mg/kg of ASO were used, and ASO incorporation into human leukocytes within the brain, bone marrow, blood, gut, liver, and spleen was assessed from 5 to 72 h later (Figure 1B). Doses and time points in this study were based on small pilot experiments in Balb/c mice that revealed similar high-frequency uptake into leukocytes (B.Z.P. and A.K., unpublished data). Live human leukocytes isolated from the tissues of mice receiving the *ACTB* ASO treatment were identified using a human-specific anti-human CD45 antibody, followed by assessment for the dequenched fluorescent signal above that of the vehicle-control-treated animals, indicating cellular uptake and hybridization of the ASO to human *ACTB* mRNA (Figure 1C).

A 1 mg/kg *ACTB* ASO dose resulted in maximal cellular and tissue penetration

In order to determine the lowest dose of the homo-doubly labeled *ACTB* ASO that would provide maximal penetration into human leukocytes within multiple mouse tissues of interest, animals were injected intravenously with either 0 mg/kg (vehicle control), 0.5 mg/kg, 1.0 mg/kg, or 2.0 mg/kg of the homo-doubly labeled *ACTB* ASO. Five hours after administration, animals were euthanized, and blood, bone marrow, liver, and spleen were collected.

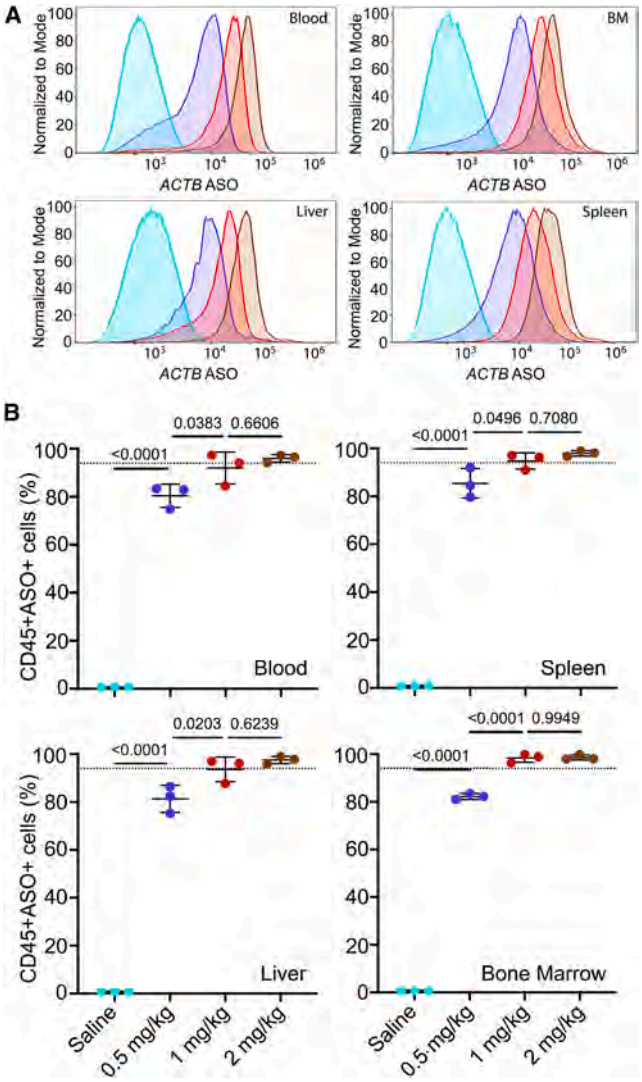

Figure 2. Dose-dependent ASO penetration into human leukocytes within multiple tissues

Humanized mice were injected intravenously with 0 mg/kg (vehicle control), 0.5 mg/kg, 1 mg/kg, or 2 mg/kg of *ACTB* ASO (n = 3 mice per group). Five hours later, mice were euthanized and human CD45$^+$ leukocytes isolated from blood, liver, bone marrow (BM), and spleen. (A) Representative histograms showing dose-dependent changes in *ACTB* ASO fluorescence. Vehicle control (turquoise), 0.5 mg/kg (purple), 1 mg/kg (red), 2 mg/kg (brown). (B) Graphed frequencies of *ACTB*-ASO-positive human leukocytes isolated from tissues at each dose. Mean with standard deviation. Dotted line is at 94%. Each dot represents data from an individual mouse. One-way ANOVA with Tukey's post-test.

Leukocytes were isolated from tissues and analyzed by flow cytometry for the presence of a fluorescent signal indicating ASO hybridization to *ACTB* mRNA in human CD45$^+$ cells. Representative flow cytometry histograms show a dose-dependent increase in the median fluorescence intensity (MFI) of the ASO-Red Rover signal in human CD45$^+$ cells isolated from the blood, bone marrow, liver, and spleen (Figure 2A) of humanized mice. Comparing the results from multiple animals, it was observed that significant increases in the frequency of human CD45$^+$ *ACTB* ASO$^+$ leukocytes plateaued at medians of $\geq$94% using a dose of 1 mg/kg for all the tissues assessed (Figure 2B). Analysis of human CD45$^-$ leukocytes (of mouse origin) demonstrated ASO penetration into non-human cells but limited binding and fluorescence as expected due to the 64% homology of the ASO sequence to murine *ACTB* (Figure S1). These results suggested that a 1 mg/kg dose of *ACTB* ASO resulted in maximal cellular and tissue penetration *in vivo*. Additionally, toxicity studies in normal, non-humanized mice indicated no apparent macroscopic, clinical, or direct toxicity findings using doses between 0.5 and 10 mg/kg, suggesting good potential for clinical translation of the 1 mg/kg dose (Table S1).

The fluorescent, hybridized *ACTB* ASO signal localized to the intracellular perinuclear space of human leukocytes

In order to determine the intracellular localization of the fluorescent *ACTB* ASO signal, animals were injected with 1 mg/kg of homo-doubly labeled *ACTB* ASO and then euthanized 5 h later. Total leukocytes isolated from the spleen were antibody stained with anti-human CD45-FITC and the DNA stain DAPI. The fluorescent *ACTB* ASO signal could be detected in association with the majority of human CD45$^+$ cells, in concordance with the flow cytometry data, and was clearly detectable residing inside the cell in the cytoplasm of CD45-FITC$^+$ cells (Figure 3, top panels). No fluorescent *ACTB* ASO signal was detectable in any cells of vehicle-control-treated animals (Figure 3, bottom panels). Z-stack imaging confirmed that the fluorescent *ACTB* ASO signal originated in the perinuclear space of the cytoplasm and was not localized within the nucleus or on the surface of cells (Video S1).

ACTB ASO tissue dissemination and persistence within target cells

Antisense nucleotides are known to preferentially accumulate in organs such as the liver and spleen,[20] which could result in greater saturation of target cells in these organs compared to cells in other organs at similar ASO doses. Thus, we assessed if the frequency of human leukocytes containing fluorescent hybridized *ACTB* ASO differed among different tissue reservoirs at the same 1 mg/kg dose. Mice were once again treated with 1 mg/kg homo-doubly labeled *ACTB* ASO and euthanized 5 h later. When comparing the frequency of CD45$^+$ human cells positive for *ACTB* ASO in blood, liver, bone marrow, and spleen, no significant differences were observed among the four tissue types (Figure 4A). We also observed that the human-specific *ACTB* ASOs could non-specifically enter human CD45$^-$ cells (of murine origin) isolated from the same four tissues and interact with murine *Actb* transcripts, resulting in fluorescence, albeit in a lower frequency of cells, likely due to reduced homology (64%) of the ASO with the murine sequence (Figure S1). In addition, we assessed the quantity of hybridized fluorescent *ACTB* mRNA ASOs in leukocytes isolated from each tissue and observed that the median fluorescent intensity of the fluorescent ASO-Red Rover signal did not differ in leukocytes regardless of whether they were isolated from blood, liver, bone marrow, or spleen (Figure 4B).

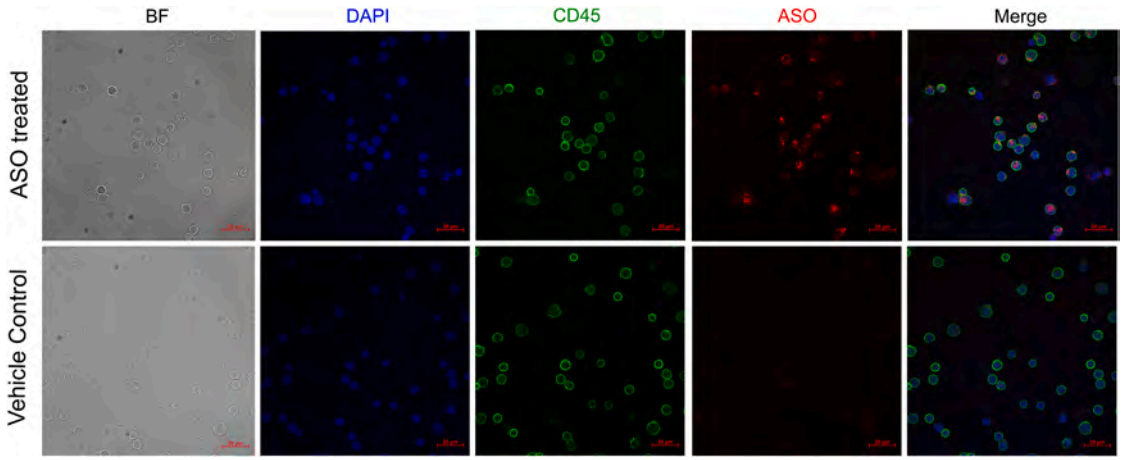

Figure 3. *ACTB* ASO is primarily localized within in the perinuclear space of human CD45⁺ leukocytes

Total splenic leukocytes isolated from humanized mice 5 h after intravenous injection with homo-doubly labeled *ACTB* ASO (top) or vehicle control (bottom) were stained with anti-human-specific CD45-FITC antibody and DAPI prior to confocal imaging. Hybridized *ACTB* ASO (red), human CD45 (green), DAPI (blue), BF (bright field). Scale bars, 20 μm. See also Video S1.

Therefore, results suggested that the *ACTB* ASO disseminated to and accumulated similarly within target cells in these four organs.

After determining that the *ACTB* ASO disseminated similarly in multiple tissue types, we then wanted to evaluate the persistence of the fluorescent *ACTB* ASO signal over a 72 h period. To accomplish this, we injected animals with 1 mg/kg of homo-doubly labeled *ACTB* ASO, then euthanized at 5, 24, 48, or 72 h post-treatment. Human CD45$^+$ cells were isolated from blood, bone marrow, liver, and spleen and analyzed by flow cytometry. At 48 h post-injection, there was a significant reduction in the percentage of CD45$^+$ cells positive for the *ACTB* ASO signal in blood, liver, and spleen (Figure 4C). However, bone marrow did not have a significant reduction in the frequency of cells positive for *ACTB* ASO until 72 h post-injection (Figure 4C). At 72 h, a median of >50% of cells remained positive for the *ACTB* ASO signal in all tissues assessed.

ACTB ASO treatment reduced levels of *ACTB* mRNA transcripts *in vivo*

To determine if a single injection of 1 mg/kg of homo-doubly labeled *ACTB* ASO could impact levels of mRNA transcripts from the *ACTB* gene that encodes for β-actin, we used RT-qPCR to assess the relative amounts of *ACTB* mRNA transcripts at 5, 24, 48, or 72 h post-treatment. Total leukocytes were isolated from bone marrow, liver, and spleen and depleted of mouse cells using anti-mouse CD45- and Ter-119-specific beads. The level of *ACTB* mRNA in the enriched human cells was then determined relative to housekeeping gene *GAPDH*. Interestingly, we found that mean relative *ACTB* transcript levels were significantly reduced at 24 h post-treatment in human cells isolated from bone marrow and remained significantly lower until at least 72 h (Figure 5A) compared to cells from vehicle-control-treated animals. In contrast, the average relative levels of *ACTB* transcripts remained unchanged in human cells isolated from liver (Figure 5B) and spleen (Figure 5C) after a single treatment. Thus, a homo-doubly labeled *ACTB* ASO demonstrated the potential to reduce the relative abundance of a target transcript.

The *ACTB* ASO penetrated difficult-to-access brain and gut tissues

Having determined that the 1 mg/kg dose of *ACTB* ASO effectively saturated leukocytes within a wide range of easily penetrated tissues and had functional capacity to reduce mRNA transcripts *in vivo* in the bone marrow, we then assessed penetration of hard-to-reach but clinically important tissues such as the brain and gut. Animals were injected intravenously with 1 mg/kg of homo-doubly labeled *ACTB* ASO, and 5 h after treatment animals were euthanized and brain and gut tissues collected. Due to low frequencies of human leukocytes in brain and gut of humanized mice, isolated leukocytes were combined from two to three individual mice and then analyzed by flow cytometry for the presence and abundance of hybridized fluorescent *ACTB* ASO within human CD45$^+$ cells. Representative histograms of CD45$^+$ *ACTB* ASO$^+$ cells in both brain and gut are shown in Figure 6A. A largely bimodal fluorescence pattern in brain was observed in five separate experiments, with a mean of 50.9 (7.9)% of the human CD45$^+$ cells taking up the *ACTB* ASO. In contrast, fluorescent *ACTB* ASO signal found in the leukocytes in the gut was largely a single population, with a mean of 66.7 (34)% human CD45$^+$ cells containing hybridized *ACTB* ASO in three separate experiments. Additionally, both brain and gut had a considerable increase in the percentage of CD45$^+$ *ACTB* ASO$^+$ cells when compared with vehicle controls (Figure 6B). To ensure that the fluorescent *ACTB* ASO$^+$ leukocytes detected in the brain were not solely residing in the vasculature as opposed to the brain parenchyma, we perfused the mice prior to brain tissue collection. An example of brain results using combined cells from perfused animals is shown by the open symbols in Figure 6B. Thus, we confirmed that the homo-doubly

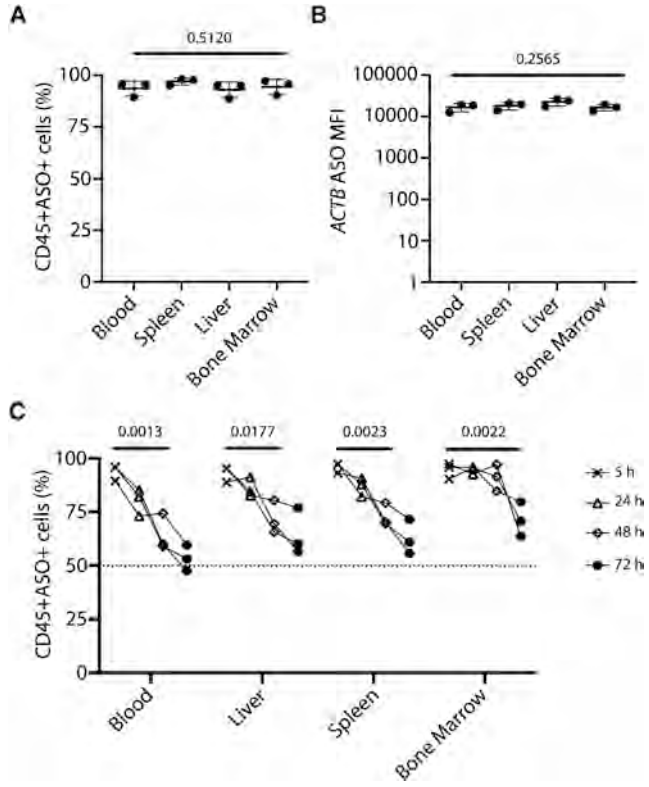

Figure 4. The *ACTB* ASO disseminated equally to target cells within multiple tissues and persisted in >50% cells over a period of 72 h

Humanized mice were injected intravenously with 1 mg/kg of the *ACTB* ASO (n = 3 mice per group) and euthanized 5 h later. Human CD45$^+$ cells isolated from blood, spleen, liver, and bone marrow were then assessed for the (A) frequency and (B) MFI of *ACTB* ASO fluorescing cells. Each dot represents an individual mouse. Mean with standard deviation. One-way ANOVA with Tukey's post-test. (C) Humanized mice were injected intravenously with 1 mg/kg of the *ACTB* ASO (n = 3 mice per time point). The frequencies of human CD45$^+$ cells positive for hybridized *ACTB* ASO in tissues were assessed at 5, 24, 48, and 72 h post-injection. Each dot represents an individual mouse. One-way ANOVA with Dunnett's post-test.

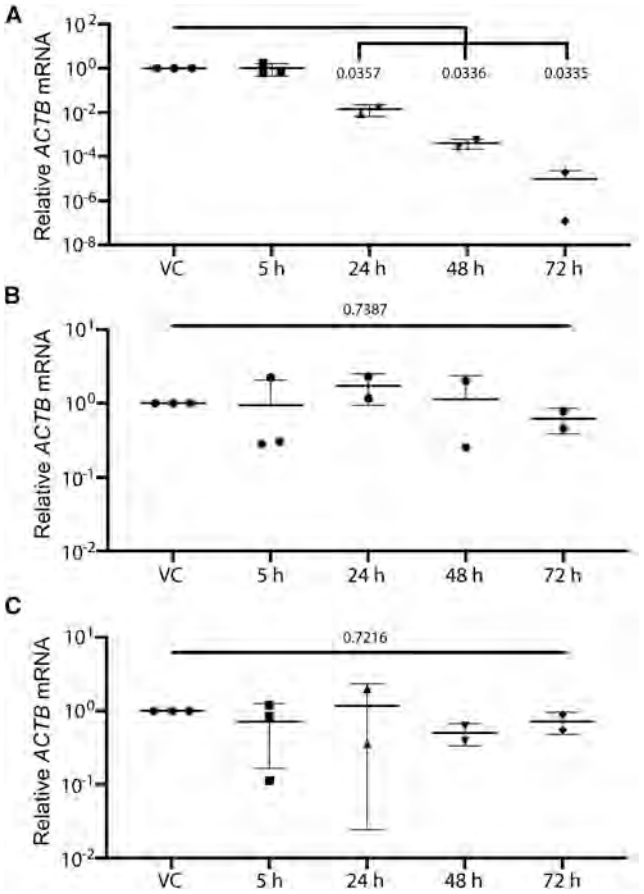

Figure 5. Administration of the homo-doubly labeled *ACTB* ASOs reduced levels of *ACTB* mRNA transcripts in human leukocytes isolated from bone marrow

Humanized mice were injected intravenously with 1 mg/kg of the *ACTB* ASO. Mice were euthanized at 5, 24, 48, and 72 h post-treatment and relative *ACTB* mRNA levels assessed in human CD45$^+$ leukocytes isolated from (A) bone marrow, (B) liver, and (C) spleen. Each dot represents data from an individual mouse. Mean with standard deviation. One-way ANOVA with Dunnett's post-test.

labeled *ACTB* ASO was also able to successfully penetrate hard-to-treat brain and gut tissues to hybridize with complementary sequences and fluoresce within human leukocytes.

The *ACTB* ASO is taken up into brain CD4$^+$ T cells with similar efficiency as other leukocytes

We anticipate using the homo-doubly labeled ASO technology to develop a new class of drugs for treatment of HIV. Since the *ACTB* ASO was detected in nearly 100% of leukocytes in most tissues, we could be assured that human CD4$^+$ T cells, the primary target of HIV infection, were taking up the ASOs. However, we needed to confirm that CD4$^+$ T cells in brain were among the cells containing hybridized *ACTB* ASO. An extended flow cytometry gating strategy was used to identify hybridized *ACTB* ASO in CD4$^+$ T cells (Figure 7A). We first assessed the frequency of CD4$^+$ T cells in the brain containing fluorescent hybridized ASO 5 h after administration of 1 mg/kg of homo-doubly labeled *ACTB* ASO compared to vehicle control. Assessment of multiple animals (n = 5), including a set of perfused animals (open symbols), indicated that the homo-doubly labeled *ACTB* ASO was incorporated into 43.1 (11.3)% of CD4$^+$ T cells in the brain (Figure 7B). Comparing *ACTB* ASO incorporation into CD4$^+$ T cells versus total CD45$^+$ leukocytes indicated there was no significant difference in the uptake of the homo-doubly labeled *ACTB* ASO by CD4$^+$ T cells compared to total leukocytes (Figure 7C).

DISCUSSION

The therapeutic potential of oligonucleotides has been hampered by the lack of effective *in vivo* delivery vehicles. The specific goal of this project has been to gather sufficient *in vivo* data to support future therapeutic applications requiring delivery of oligonucleotides into

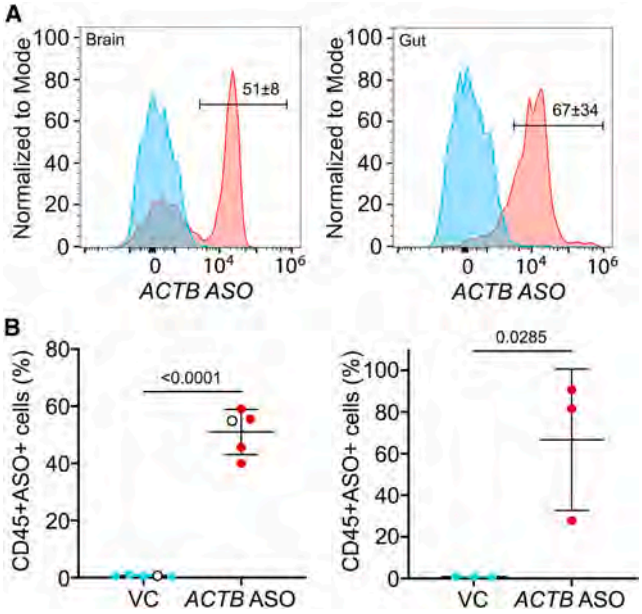

Figure 6. The homo-doubly labeled *ACTB* ASO penetrates into hard-to-reach brain and gut tissues

Humanized mice were injected intravenously with 1 mg/kg of the *ACTB* ASO. Five hours post-injection, mice were euthanized and human CD45$^+$ leukocytes isolated from brain and gut. (A) Representative histograms showing homo-doubly labeled *ACTB* ASO fluorescence in human leukocytes isolated from brain and gut. More than 50 LIVE/DEAD$^-$CD45$^+$ events were collected for assessment of ASO incorporation. No differences in leukocyte yield was observed between vehicle-control- or ASO-treated animals. (B) Collated frequencies of *ACTB* ASO$^+$ human CD45$^+$ leukocytes isolated from brain (n = 5) and gut (n = 3) tissue. Each dot represents a separate experiment using leukocytes combined from two to three individual mice. Mean with standard deviation. Open symbols indicate perfused animals. Unpaired t test.

hematopoietic cells within specific tissues. Thus, we now present data from six tissues from a humanized mouse model system where an ASO bearing an H-type excitonic dimer complementary to human β-actin (*ACTB*) mRNA has been delivered into human leukocytes without toxicity. We have previously used this molecular design to successfully demonstrate delivery of fluorogenic protease substrates and fluorogenic oligonucleotide probes into cells in culture. In these earlier studies, the entry of these probes into cells has been consistent with passive diffusion, eliminating the need for carriers such as lipids, e.g., liposomes and nanoparticles, or receptor-ligand conjugates, e.g., GalNAc-siRNAs, and concerns of entrapment within endosomes.[12,13]

As we are particularly interested in development of therapy for HIV patients, we have focused on CD45$^+$ and specifically CD4$^+$ cells in blood and tissues that support HIV infection. Use of customized oligonucleotide therapy could be beneficial to patients who have failed the now standard combined antiretroviral therapy (cART). Additionally, the functional knockdown of residual mRNA transcription from HIV provirus is a promising new approach to alleviate the persistent inflammation that drives morbidity in patients despite effective cART.[21–24] Other applications include treatment of other infectious diseases in which lymphocytes are infected or tumorigenic, metastatic tumor cells dispersed in tissues, and neurodegenerative disorders in which the target gene expression has been known for some time such as Alzheimer disease but no effective genetic-based therapy has been successful.[25]

In this study, we synthesized a homo-doubly labeled probe specific for the mRNA coding for the ubiquitously expressed human β-actin (*ACTB*) gene and assessed its delivery into hematopoietic cells, which are notoriously resistant to ASO delivery.[8] Using a humanized mouse model, we observed the induction of a fluorogenic signal upon ASO hybridization with its complementary genetic sequence in leukocytes from six different tissues *in vivo* using both flow cytometry and confocal microscopy. Confocal examination of human leukocytes isolated from mouse spleens indicated the fluorogenic signals from hybridized ASOs originated in the perinuclear space. This intracellular signal, combined with a lack of surface staining, is consistent with passive diffusion of the ASOs without endosomal involvement, supports the potential for mRNA degradation or translation blockade, and is consistent with our previous findings *in vitro*.[13] While delivery of ASO to cells is commonly highly cytotoxic,[8,9] confocal imaging (Figure 3) and viability staining followed by flow cytometric analysis (Figure 1C) suggested little to no toxicity to cells containing the ASO in the humanized mouse.

We assessed the dose-dependent delivery of the homo-doubly labeled *ACTB* ASO into CD45$^+$ cells in the blood, bone marrow, liver, and spleen at doses ranging between 0.5 and 2 mg/kg. In each case there was a four to five log increase in intensity over vehicle control for the *ACTB* ASO signal. Saturation of signal occurred at a dose of 1 mg/kg, which is equivalent to a 12.3 mg/kg dose in humans[26] and is well within the dose range of other approved oligonucleotide-based therapeutics.[4] Indeed, no morbidity or other adverse effects were observed in the mice over the duration of the study, which was consistent with the toxicity assessments we performed in normal non-humanized mice (Table S1). Significantly, the homo-doubly labeled *ACTB* ASOs disseminated equally as indicated by the percentage of ASO$^+$CD45$^+$ cells and the MFIs in the target cells within the blood, spleen, liver, and bone marrow. Non-specific cellular entry but sequence-specific hybridization and subsequent fluorescence was demonstrated by a reduced frequency of murine cells fluorescing from these same four tissues. Interestingly, although the *ACTB* ASO signal in human cells decayed differently in each of the tissues, the probe remained bound to its target sequence in >50% of cells for at least 72 h post-treatment, indicating significant resistance to cellular degradation likely due to the phosphorothioate backbone. The data showing ASO entry into hard-to-reach tissues such as brain and gut were highly promising. Unfortunately, since whole brains were required to harvest sufficient cells for flow cytometric analysis, confocal analysis of brain sections was not possible to

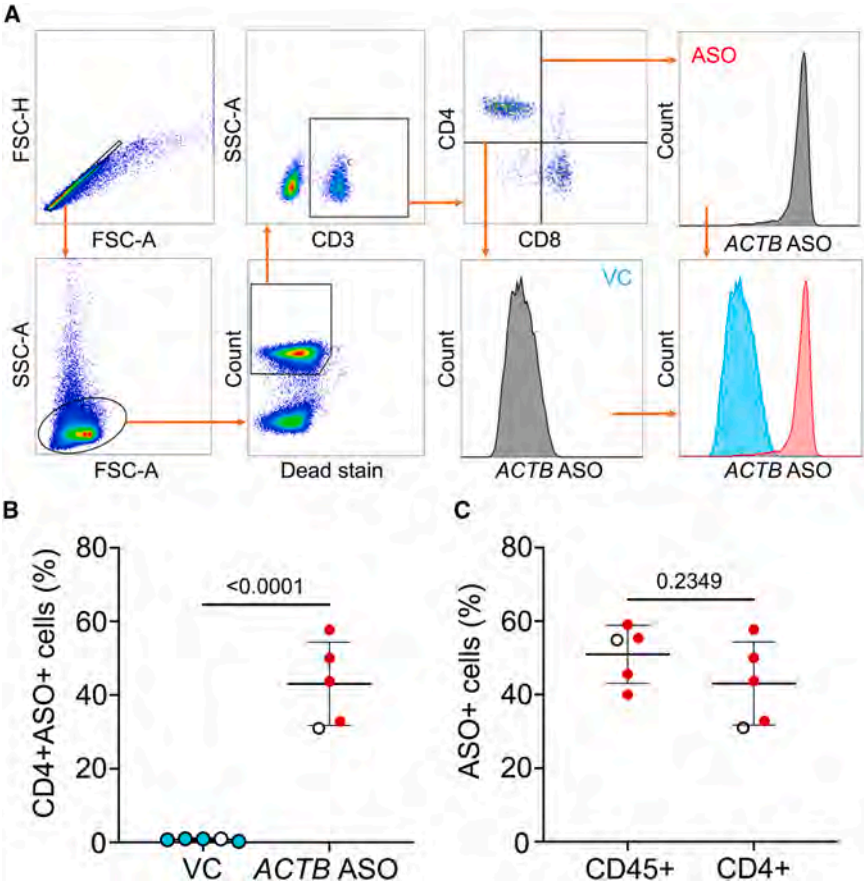

Figure 7. CD4⁺ T cells in brain uptake *ACTB* ASO as efficiently as other leukocyte subsets

Humanized mice were injected intravenously with 1 mg/kg of homo-doubly labeled *ACTB* ASO. Five hours post-injection, mice were euthanized and human leukocytes assessed by flow cytometry for the presence of hybridized ASO. (A) Representative flow cytometry plots gating on live human CD4⁺ T cells and assessment of fluorescence within cells from treated (ASO) or vehicle control (VC) animals. More than 50 LIVE/DEAD⁻CD45⁺CD3⁺CD4⁺ events were collected for assessment of ASO incorporation. No differences in leukocyte yield was observed between vehicle-control- or ASO-treated animals. Collated frequencies of *ACTB* ASO⁺ human CD4⁺ T cells in comparison with (B) vehicle controls (VC) or (C) CD45⁺ leukocytes isolated from brain (n = 5) tissue. Each dot represents a separate experiment using leukocytes combined from two to three mouse brains. Mean with standard deviation. Open symbols indicate data from perfused animals. Unpaired t test.

confirm the perfusion results that supported the conclusion that the ASOs were accessing leukocytes within the brain parenchyma and not solely within the vasculature. Additionally, although the low cell numbers inherent to the tissue compartments and humanized model prevented assessment of the individual variability of ASO incorporation into leukocytes within the brain and gut, we were able to identify a range of ASO infiltration over at least nine different animals per tissue.

Intriguingly, we found the major difference among the four tissues was at the *ACTB* transcript level. A significant reduction in *ACTB* transcripts was detected by 24 h post-treatment in human cells isolated from the bone marrow, and this decrease remained significantly lower for at least 72 h compared to cells from untreated animals. In contrast, relative levels of *ACTB* transcripts remained statistically unchanged in human cells isolated from the liver and spleen after a single treatment. Notably, the suppression of *ACTB* transcripts in bone marrow was associated with a greater frequency of cells retaining hybridized *ACTB* ASO over time in this tissue, which may have related to the greater effect on *ACTB* transcripts in bone marrow. Leukocytes in the bone marrow are more transcriptionally active due to their rapid division and differentiation[27] than leukocytes found in spleen and liver under healthy conditions. The β-actin protein is crucial for these processes,[28] and thus, more active *ACTB* transcription in bone marrow leukocytes may have facilitated detection of its knockdown compared to other tissues. Future studies are planned to address tissue-specific differences in gene suppression and devise optimal ASO regimens to suppress target transcripts across relevant tissues. Overall, the *ACTB* ASO formulation demonstrated the capacity to functionally suppress cellular mRNA transcripts *in vivo* particularly in bone marrow leukocytes where the rate of cell division is quite high.

We were particularly interested in the delivery of the *ACTB* ASO into the CD4⁺ T cells that are the cellular targets of HIV infection. In the majority of tissues assessed, the *ACTB* ASO could be detected in over 90% of leukocytes, suggesting ample penetration into CD4⁺ T cells. However, incorporation into CD45⁺ cells within the brain was significantly lower, requiring us to specifically assess incorporation into CD4⁺ T cells. We found the same low 1 mg/kg dose resulted in a significant frequency of CD4⁺ T cells containing hybridized *ACTB* ASO that did not differ significantly from total CD45⁺ brain leukocytes, suggesting high applicability of the technology for delivery of ASOs that target HIV sequences to multiple clinically relevant tissues, including hard-to-treat brain tissues, *in vivo*. In none of the experiments did we see a differential effect of mouse or human donor sex on results, suggesting the delivery system would be broadly effective in both sexes.

In summary, this study portends well for the use of our new molecular design for the *in vivo* delivery of fluorogenic oligonucleotide probes for therapeutic applications.

MATERIALS AND METHODS

Antisense oligonucleotide

The non-gapmer ASO sequence for the housekeeping gene *ACTB* (β-actin) was comprised of the following 24-nucleotide sequence 5′-CGCGGCGATATCATCATCCATAAC-3′, with phosphorothioate internucleotide linkages throughout terminating with deoxythymidine and a six-carbon spacer and an amino group in the 5′ position on both ends. The amino groups on the ends of the ASO were reacted with the same succinimidyl fluorophore, Red Rover (OncoImmunin, Inc., Gaithersburg, MD) (to be read in the APC channel) as used previously, resulting in homo-doubly labeling, then purified by reverse phase HPLC, lyophilized, and resuspended in phosphate-buffered saline (PBS) as previously described.[13] The presence of an H-type excitonic dimer in each ASO was confirmed by spectrophotometry.[16]

Toxicity assessment

Male 6- to 8-week-old B6C3F1 mice were dosed with vehicle, 0.5, 2.0, or 10 mg/kg of homo-doubly labeled phosphorothioate ASO (five mice per group) via the tail vein. Gross necropsy to collect spleens and livers and blood collection were performed after 24 h of the 10 mg/kg dose and 7 days after injection for all doses (five groups total). The ratio of AST/ALT and total white and red cell counts were assessed in blood. Spleens and livers were scored for histopathology using the grading scale 0 = no notable findings; 1 = focal, minimal degree; 2 = diffuse, minimal degree; 3 = diffuse, mild degree for three separate parameters per sample.

Humanization and ASO treatment of mice

Triple knockout mice were humanized using the BLT method as previously described.[18,19] Briefly, 6- to 10-week-old mice were irradiated with 4.5 Gy before transplantation of 17- to 22-week-gestation human liver and thymus under the kidney capsule followed by injection of autologous $CD34^+$ progenitor cells. Mice were housed under specific pathogen-free conditions. To control for sex and donor differences, male and female humanized mice generated from four human donors of both sexes were used in experiments. Mice were matured for >12 weeks and were reconstituted with $\geq 2 \times 10^5$ human $CD45^+$ cells/mL of blood. β-actin-specific ASOs were diluted in 0.9% sodium chloride (Baxter, Mississauga, Canada) prior to intravenous injection. Animal studies were performed under University of Saskatchewan's Animal Research Ethics Board protocols 20180079 and 20220025 and adhered to Canadian Council on Animal Care guidelines. Human tissues were obtained through anonymous donations with informed consent via a US-based tissue procurement partner under the University of Saskatchewan Research Ethics Board Bio ID-371.

Human leukocyte isolation

Blood was collected into 0.5 M EDTA, diluted in saline (Baxter), and leukocytes isolated following density centrifugation using Histopaque 1077 (Sigma-Aldrich, St. Louis, MO). Thymic organoid, lymph node, spleen, liver, and brain were all directly passed through 70-μm filters and bone marrow flushed from the long bones of the leg using R-10 medium (RPMI-1640 (Cytiva, Marlborough, MA), 10% fetal bovine serum (FBS; Thermo Fisher Scientific, San Diego, CA), 100 μg/mL Penicillin/Streptomycin (Gibco, Amarillo, TX), and 1 mM L-Glutamine (Cytiva). Red blood cell (RBC) lysis buffer (BioLegend, San Diego, CA) was used to lyse residual red cells from spleen and bone marrow. Liver and brain leukocytes were further purified by density purification using Percoll (Sigma-Aldrich, St. Louis, MO). Gut leukocytes were harvested by similarly digesting PBS (Gibco)-flushed and sectioned intestines before passing supernatant through a 70-μm cell strainer and purification by Percoll gradient.

Flow cytometry staining

Isolated leukocytes were stained with LIVE/DEAD Fixable Red Dead Cell Stain Kit (Thermo Fisher) and anti-human CD45-eFluor506 (Clone HI30; Thermo Fisher), CD3-eFluor450 (Clone UCHT1; Thermo Fisher), CD4-PE-Cy7 (Clone RPA-T4; Thermo Fisher), and CD8-BV605 (Clone SK1; BD Biosciences, San Jose, CA) for 15 min at 4°C in the dark before washing with cold PBS (Cytiva) containing 2% FBS (Thermo Fisher). Samples were fixed with 2% paraformaldehyde (Sigma-Aldrich) before analysis on a CytoFLEX (V5-B5-R3) flow cytometer (Beckman Coulter, Brea, CA). Data analysis was performed using FlowJo 10.10.0 software (BD Biosciences).

Quantitative RT-PCR

Isolated leukocytes were depleted of mouse cells by negative selection using anti-mouse CD45 and Ter-119 microbeads (Miltenyi, Gaithersburg, MA). Then, RNA was isolated from a maximum of 500K human leukocytes using a RNease mini-isolation kit (Qiagen, Hilden, Germany). Relative levels of *ACTB* mRNA were determined using iTaq Universal SYBR Green One Step Kit (BioRad) with glyceraldehyde-3-phosphate dehydrogenase (*GAPDH*) as a housekeeping control. In brief, 40 ng of RNA was added to 20 μL of iTaq master mix containing 250 nM primers for either *ACTB* (FP: 5′ AGAGCTACGAGCTGCCTGAC 3'; RP 5′ AGTACTTGCGCTC AGGAGGA 3'; annealing temperature 63°C) or *GAPDH* (FP 5′ CCACAGTCCATGCCATCACT 3'; RP 5′ ATGCCAGTGAGCTT CCCG 3'; annealing temperature 55°C). Sample runs followed manufacturer's recommended program for a Step One Plus thermal cycler (Applied Biosystems, Waltham, MA). Relative gene expression was calculated using $2^{-\Delta\Delta CT}$.

Confocal imaging

Leukocytes isolated from mice were stained with anti-human CD45-A488 antibody (Clone HI30; BioLegend) as described in the flow cytometry staining section. Cells were fixed in 2% paraformaldehyde (PFA) (Sigma-Aldrich) for a minimum of 2 h, then resuspended in 200 μL of PBS (Cytiva), and stored in the dark at 4°C. Samples were mounted on Superfrost Plus microscope slides using a Cytospin 4 (Thermo Fisher). In brief, prepared samples were centrifuged at 70 *x* g for 3 min, then sealed with DAPI-containing ProLong Diamond Antifade self-sealing mountant (Thermo Fisher) and a coverslip (Thermo Fisher). Imaging was performed

on a Zeiss LSM 700 microscope utilizing ZEN Black software (Zeiss, Oberkochen, Germany). Microscope settings were identical for all image collection.

Graphing and statistical analysis

Shapiro-Wilk test of normality and parametric one-way ANOVA with Tukey's or Dunnett's multiple comparisons test were performed. $p < 0.05$ was considered statistically significant. Statistics were performed using Prism 10.2.2 (GraphPad, San Diego, CA).

DATA AVAILABILITY

The data and materials that support the findings of this study are available from the corresponding authors (B.Z.P. or K.J.L.) upon reasonable request.

ACKNOWLEDGMENTS

Support for this work was supplied by the Canadian Institutes of Health Research (PJT-183929) and OncoImmunin, Inc. Special thanks to Dr. Akira Komoriya for contributions to the initial oligonucleotide selection, Dr. Pashupati Bhandari for technical assistance, and Satyajit Biswas and Madeline T.E. Stewart for production of humanized mice used in the study.

AUTHOR CONTRIBUTIONS

K.J.L. and B.Z.P. conceptualized the study and directed the methodology; K.J.L. supervised the work; N.B.S. and S.S.R. generated and N.B.S. analyzed the data; N.B.S., B.Z.P., and K.J.L. wrote and edited the manuscript.

DECLARATION OF INTERESTS

B.Z.P. and A.K. are the inventors of the fluorogenic technology using H-type excitonic structures described in this manuscript (Publication number: 20240401040) and own stock in OncoImmunin, Inc.

SUPPLEMENTAL INFORMATION

Supplemental information can be found online at https://doi.org/10.1016/j.omtm.2025.101583.

REFERENCES

1. Cheng, X., and Lee, R.J. (2016). The role of helper lipids in lipid nanoparticles (LNPs) designed for oligonucleotide delivery. Adv. Drug Deliv. Rev. *99*, 129–137. https://doi.org/10.1016/j.addr.2016.01.022.

2. Dowdy, S.F., Setten, R.L., Cui, X.S., and Jadhav, S.G. (2022). Delivery of RNA Therapeutics: The Great Endosomal Escape. Nucleic Acid Ther. *32*, 361–368. https://doi.org/10.1089/nat.2022.0004.

3. Mangla, P., Vicentini, Q., and Biscans, A. (2023). Therapeutic Oligonucleotides: An Outlook on Chemical Strategies to Improve Endosomal Trafficking. Cells *12*, 2253. https://doi.org/10.3390/cells12182253.

4. Egli, M., and Manoharan, M. (2023). Chemistry, structure and function of approved oligonucleotide therapeutics. Nucleic Acids Res. *51*, 2529–2573. https://doi.org/10.1093/nar/gkad067.

5. Hammond, S.M., Aartsma-Rus, A., Alves, S., Borgos, S.E., Buijsen, R.A.M., Collin, R.W.J., Covello, G., Denti, M.A., Desviat, L.R., Echevarría, L., et al. (2021). Delivery of oligonucleotide-based therapeutics: challenges and opportunities. EMBO Mol. Med. *13*, e13243. https://doi.org/10.15252/emmm.202013243.

6. Nedorezova, D.D., Dubovichenko, M.V., Belyaeva, E.P., Grigorieva, E.D., Peresadina, A.V., and Kolpashchikov, D.M. (2022). Specificity of oligonucleotide gene therapy (OGT) agents. Theranostics *12*, 7132–7157. https://doi.org/10.7150/thno.77830.

7. Roberts, T.C., Langer, R., and Wood, M.J.A. (2020). Advances in oligonucleotide drug delivery. Nat. Rev. Drug Discov. *19*, 673–694. https://doi.org/10.1038/s41573-020-0075-7.

8. Ohyagi, M., Nagata, T., Ihara, K., Yoshida-Tanaka, K., Nishi, R., Miyata, H., Abe, A., Mabuchi, Y., Akazawa, C., and Yokota, T. (2021). DNA/RNA heteroduplex oligonucleotide technology for regulating lymphocytes in vivo. Nat. Commun. *12*, 7344. https://doi.org/10.1038/s41467-021-26902-8.

9. Le Grice, S.F.J. (2015). Targeting the HIV RNA genome: high-hanging fruit only needs a longer ladder. Curr. Top. Microbiol. Immunol. *389*, 147–169. https://doi.org/10.1007/82_2015_434.

10. Packard, B.Z., Toptygin, D.D., Komoriya, A., and Brand, L. (1996). Profluorescent protease substrates: intramolecular dimers described by the exciton model. Proc. Natl. Acad. Sci. USA *93*, 11640–11645. https://doi.org/10.1073/pnas.93.21.11640.

11. Packard, B.Z., Toptygin, D.D., Komoriya, A., and Brand, L. (1997). Design of profluorescent protease substrates guided by exciton theory. Methods Enzymol. *278*, 15–23. https://doi.org/10.1016/s0076-6879(97)78004-2.

12. Packard, B.Z., and Komoriya, A. (2008). A method in enzymology for measuring hydrolytic activities in live cell environments. Methods Enzymol. *450*, 1–19. https://doi.org/10.1016/S0076-6879(08)03401-0.

13. Packard, B.Z., Wrightson, J.A., Jr., and Komoriya, A. (2020). An Oligonucleotide Delivery Platform to Enable Assessment of Intracellular Transcripts in Live Cells by Flow Cytometry. Cytometry. A. *97*, 945–954. https://doi.org/10.1002/cyto.a.24174.

14. Reyes-Darias, J.A., Sánchez-Luque, F.J., and Berzal-Herranz, A. (2012). HIV RNA dimerisation interference by antisense oligonucleotides targeted to the 5' UTR structural elements. Virus Res. *169*, 63–71. https://doi.org/10.1016/j.virusres.2012.07.004.

15. Packard, B.Z., Toptygin, D.D., Komoriya, A., and Brand, L. (1998). Intramolecular Resonance Dipole−Dipole Interactions in a Profluorescent Protease Substrate. J. Phys. Chem. B *102*, 752–758. https://doi.org/10.1021/jp972845b.

16. Packard, B.Z., and Komoriya, A. (2025). The Influence of Length and Sequence of Complementary Oligonucleotides on the Spectral and Time-Resolved Fluorescence Properties of an H-Type Excitonic Dimer-Bearing Antisense Oligonucleotide. J. Phys. Chem. B *129*, 684–691. https://doi.org/10.1021/acs.jpcb.4c07517.

17. Komoriya, A., Packard, B.Z., Brown, M.J., Wu, M.L., and Henkart, P.A. (2000). Assessment of caspase activities in intact apoptotic thymocytes using cell-permeable fluorogenic caspase substrates. J. Exp. Med. *191*, 1819–1828. https://doi.org/10.1084/jem.191.11.1819.

18. Lavender, K.J., Messer, R.J., Race, B., and Hasenkrug, K.J. (2014). Production of bone marrow, liver, thymus (BLT) humanized mice on the C57BL/6 Rag2(-/-)gammac(-/-)CD47(-/-) background. J. Immunol. Methods *407*, 127–134. https://doi.org/10.1016/j.jim.2014.04.008.

19. Lavender, K.J., Pang, W.W., Messer, R.J., Duley, A.K., Race, B., Phillips, K., Scott, D., Peterson, K.E., Chan, C.K., Dittmer, U., et al. (2013). BLT-humanized C57BL/6 Rag2-/-gammac-/-CD47-/- mice are resistant to GVHD and develop B- and T-cell immunity to HIV infection. Blood *122*, 4013–4020. https://doi.org/10.1182/blood-2013-06-506949.

20. Dhuri, K., Bechtold, C., Quijano, E., Pham, H., Gupta, A., Vikram, A., and Bahal, R. (2020). Antisense Oligonucleotides: An Emerging Area in Drug Discovery and Development. J. Clin. Med. *9*, 2004. https://doi.org/10.3390/jcm9062004.

21. Dornadula, G., Zhang, H., VanUitert, B., Stern, J., Livornese, L., Jr., Ingerman, M.J., Witek, J., Kedanis, R.J., Natkin, J., DeSimone, J., and Pomerantz, R.J. (1999). Residual HIV-1 RNA in blood plasma of patients taking suppressive highly active antiretroviral therapy. JAMA *282*, 1627–1632. https://doi.org/10.1001/jama.282.17.1627.

22. Imamichi, H., Smith, M., Adelsberger, J.W., Izumi, T., Scrimieri, F., Sherman, B.T., Rehm, C.A., Imamichi, T., Pau, A., Catalfamo, M., et al. (2020). Defective HIV-1 proviruses produce viral proteins. Proc. Natl. Acad. Sci. USA *117*, 3704–3710. https://doi.org/10.1073/pnas.1917876117.

23. Imamichi, H., Dewar, R.L., Adelsberger, J.W., Rehm, C.A., O'Doherty, U., Paxinos, E.E., Fauci, A.S., and Lane, H.C. (2016). Defective HIV-1 proviruses produce novel protein-coding RNA species in HIV-infected patients on combination antiretroviral therapy. Proc. Natl. Acad. Sci. USA *113*, 8783–8788. https://doi.org/10.1073/pnas.1609057113.

24. Cai, C.W., and Sereti, I. (2021). Residual immune dysfunction under antiretroviral therapy. Semin. Immunol. *51*, 101471. https://doi.org/10.1016/j.smim.2021.101471.

25. Ortega, A., Chernicki, B., Ou, G., and Parmar, M.S. (2025). From Lab Bench to Hope: Emerging Gene Therapies in Clinical Trials for Alzheimer's Disease. Mol. Neurobiol. *62*, 1112–1135. https://doi.org/10.1007/s12035-024-04285-3.

26. Nair, A.B., and Jacob, S. (2016). A simple practice guide for dose conversion between animals and human. J. Basic Clin. Pharm. *7*, 27–31. https://doi.org/10.4103/0976-0105.177703.

27. Paul, F., Arkin, Y., Giladi, A., Jaitin, D.A., Kenigsberg, E., Keren-Shaul, H., Winter, D., Lara-Astiaso, D., Gury, M., Weiner, A., et al. (2015). Transcriptional Heterogeneity and Lineage Commitment in Myeloid Progenitors. Cell *163*, 1663–1677. https://doi.org/10.1016/j.cell.2015.11.013.

28. Xie, X., Almuzzaini, B., Drou, N., Kremb, S., Yousif, A., Farrants, A.K.Ö., Gunsalus, K., and Percipalle, P. (2018). beta-Actin-dependent global chromatin organization and gene expression programs control cellular identity. FASEB J. *32*, 1296–1314. https://doi.org/10.1096/fj.201700753R.